Confinement effects on Brillouin scattering in semiconductor nanowire photonic crystal

Pierre-Adrien Mante,[1,*] Nicklas Anttu,[2] Wei Zhang,[1] Jesper Wallentin,[2] I-Ju Chen,[2] Sebastian Lehmann,[2] Magnus Heurlin,[2] Magnus T. Borgström,[2] Mats-Erik Pistol,[2] and Arkady Yartsev[1,†]

[1]*Department of Chemical Physics and NanoLund, Lund University, Box 118, 221 00 Lund, Sweden*

[2]*Department of Solid State Physics and NanoLund, Lund University, Box 118, 221 00 Lund, Sweden*

(Received 21 January 2016; revised manuscript received 30 June 2016; published 28 July 2016)

Scattering of photons by phonons, or Brillouin scattering, enables manipulation and control of light and has led to revolutionary applications, from slow light to saser and cooling of micromechanical resonators. Recently, enhanced light and sound interaction has been demonstrated in waveguides. However, the design of the waveguide geometry tunes and alters the phonon and photon dispersion simultaneously. Here we investigate, through femtosecond pump-probe spectroscopy and theoretical modeling, the light and sound interaction in a bottom-up fabricated vertical nanowire photonic crystal. In such a system, the phonon dispersion can be tuned by varying the geometry of the constituent nanowires. In contrast, the placement of the nanowires in the photonic crystal can be used for tuning optical array modes, without altering the phonon dispersion. We demonstrate the forward and backward scattering, by acoustic phonons in the nanowires, of (1) such optical array modes and (2) guided modes of the constituent nanowires. Furthermore, our results reveal an enhanced interaction of array modes with phonons that we attribute to the specific scattering mechanism. Our results enable the design of a photonic crystal with separately tailored photon and phonon dispersion for Brillouin scattering. We anticipate these advances to be a starting point for enhanced control of light at the nanoscale.

DOI: 10.1103/PhysRevB.94.024115

When the wavelengths of sound and light are comparable, photons are scattered by phonons, a phenomenon denoted Brillouin scattering [1]. Multiple experimental techniques are centered on this phenomenon. For instance, in stimulated Brillouin scattering [2–7], light induces acoustic vibrations that in turn interact with light, and in picosecond ultrasonics [8–16], a laser pulse generates a coherent phonon population that is probed thanks to a second time-delayed laser pulse. Brillouin scattering has been extensively applied to the nondestructive study of mechanical properties and phonon dynamics [14–16]. Recently, enhanced light-sound interaction was demonstrated in waveguides, enabled by the collinearity and stronger overlap of guided photon and guided phonon modes in this system [2–4]. With the prospect of miniaturized devices, researchers have investigated various effects in such waveguides, including slow light [5], single phonon counting [6], and electromagnetically induced transparency [7]. However, the design of the waveguide geometry alters simultaneously the dispersion of the guided acoustic phonons and the guided optical modes. For greater flexibility in using Brillouin scattering at the nanoscale, it is important to develop and investigate structures that allow for a more independent tuning of the phonon and photon dispersion.

Here we show how a nanowire photonic crystal (PhC) made of a square array of InP nanowires allows for strong confinement of acoustic phonons and supports multiple optical modes. In such a nanowire PhC, in addition to optical modes due to waveguiding in the constituent nanowires, a delocalized optical array mode due to coupling between the nanowires can also show up [17,18]. We verify the scattering of both types of modes with guided acoustic phonons of the nanowires using time resolved pump-probe measurements. Importantly, the nanowire diameter determines the phonon dispersion, whereas the array period can be used for tuning the dispersion of the delocalized array mode, without affecting the phonon dispersion. In this way, we open the door for independent tuning of phonons and photons for Brillouin scattering in nanostructures. In addition, the guiding of the photons by the nanowires breaks the isotropy of the phonon generation process and enables the observation of nonaxisymmetric acoustic modes that are not expected in time resolved experiments of nanostructures [13,14]. Our results demonstrate the potential of nanowire PhCs for highly engineered light manipulation by sound at the nanoscale.

For the experiments, *p*-type InP nanowires [Fig. 1(a)] were epitaxially grown by low pressure (100 mbar) metal organic vapor phase epitaxy using gold seed particles arranged in arrays defined by nanoimprint lithography, metal evaporation, and lift-off [19,20]. After growth, the metal seed particles were removed using a KI based wet chemical etching procedure.

Picosecond ultrasonics experiments [8–16] were performed using a regeneratively amplified, mode-locked Yb:KGW (ytterbium-doped potassium gadolinium tungstate) based femtosecond laser system (Pharos, Light Conversion) operating at 1030 nm and delivering pulses of 200 fs at 2 kHz repetition rate. This laser is then used to pump two noncollinearly phase-matched optical parametric amplifiers (NOPAs). A first one (Orpheus-N, Light Conversion) was used to generate pump pulses centered at 550 nm with pulse duration of 35 fs. The second NOPA (Orpheus-N, Light Conversion) generated probe pulses with about 40 fs pulse duration at wavelengths ranging from 650 to 900 nm. The pump beam was chopped at a frequency of 1 kHz using a mechanical chopper. Experiments were performed using a classical reflectivity setup either at normal or 70° incidence angle. In the picosecond ultrasonics experiments, an absorbed pump laser beam excites electrons in the nanowires, leading to generation of acoustic phonons through thermoelasticity and deformation potential [11].

*pierre-adrien.mante@chemphys.lu.se
†arkady.yartsev@chemphys.lu.se

 ©2016 American Physical Society

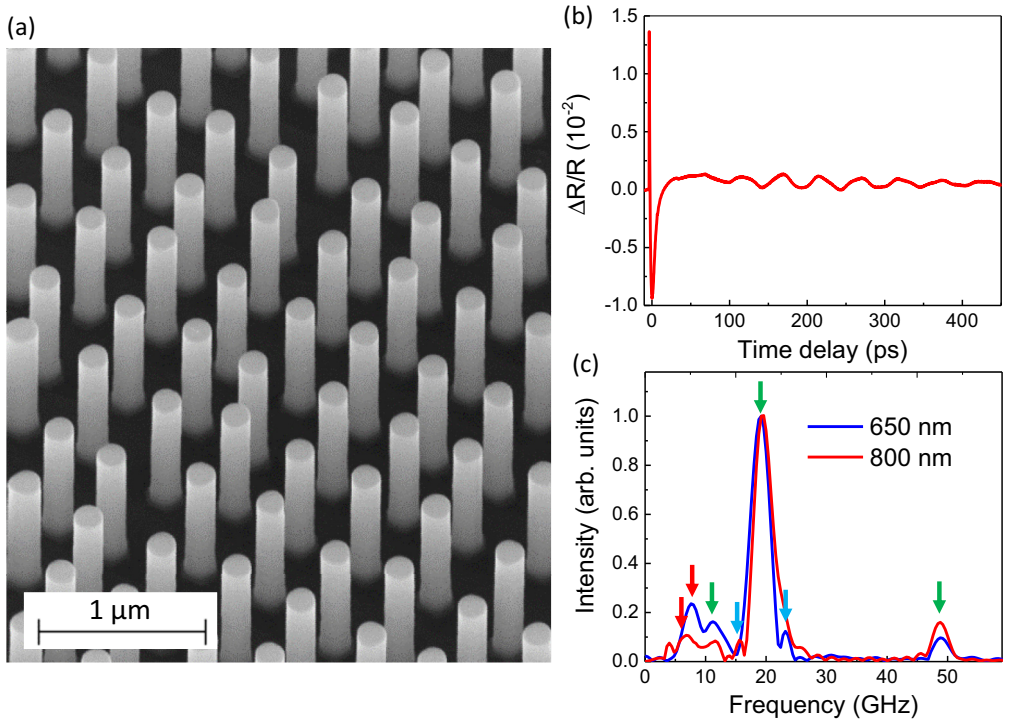

FIG. 1. (a) Scanning electron micrograph of the InP PhC. (b) Transient reflectivity trace obtained on the InP PhC for a pump wavelength λ_{pump} of 550 nm and a probe wavelength λ_{probe} of 850 nm. (c) Normalized Fourier transform of the transient reflectivity traces obtained with $\lambda_{pump} = 550$ nm and $\lambda_{probe} = 650$ nm or $\lambda_{probe} = 800$ nm. The green (red and blue) arrows points at the frequencies that are unchanged (changed) with varying probe wavelength.

A second beam, the probe, is time delayed by t with respect to the pump by a mechanical delay stage. We measure the relative transient reflectivity $\Delta R(t)/R$, where R and $R + \Delta R(t)$ represent the probe reflected by the sample with and without pump, respectively. In Fig. 1(b) we show the transient reflectivity obtained with a pump wavelength of 550 nm and a probe of 850 nm. At short time delay we observe an abrupt change in the reflectivity induced by photoexcited carriers. Then, oscillations appear due to Brillouin scattering by the pump induced coherent phonons. These oscillations are resulting from interferences between the multiple probe reflections and the Brillouin scattered probe [8].

In Fig. 1(c) we show two frequency spectra of the transient reflectivity, obtained with a probe wavelength of 650 and 800 nm. We identify a number of prominent peaks [marked by the arrows in Fig. 1(c)]. Some of these peaks shift when the probe wavelength is changed while some peaks do not. As discussed below, the peaks that shift are marked by the blue and red arrows and correspond to backward Brillouin scattering, and the other marked peaks correspond to forward Brillouin scattering.

The Brillouin scattering process occurs as follows: a photon of wave vector $\boldsymbol{k}_1$ and frequency ω_1 interacts with a phonon of wave vector $\boldsymbol{q}$ and frequency Ω to generate a scattered photon of wave vector $\boldsymbol{k}_2$ and frequency ω_2. Energy and momentum conservations dictate [1]

$$\boldsymbol{q} = \boldsymbol{k}_2 - \boldsymbol{k}_1, \tag{1}$$

$$\Omega = \omega_2 - \omega_1. \tag{2}$$

Since the frequency of the phonon is small compared to the frequency of light, we have $|\boldsymbol{k_1}| \approx |\boldsymbol{k_2}| \approx k$.

In an isolated nanowire waveguide, photons and phonons can only propagate along the nanowire axis, the scattering is thus independent of the incidence angle of the probe light, which leads to two possible cases. First, when the incident and scattered light are in the same direction (forward scattering), we have the relation $q = 0$, which corresponds to nonpropagating phonons. The scattering is thereby independent of the photon wavelength. In the second case, the incident and scattered light are in opposite directions (backward scattering), with $q = 2k$ leading thus to a strong dependence on the wavelength. In this case, propagating phonons are responsible for the scattering. In our study, thanks to the finite length of the nanowires, reflection from the nanowires-substrate interface occurs and enables the observation of both forward and backward scattering. To be able to relate the marked peaks in Fig. 1(c) to such forward and backward Brillouin scattering, we calculated both the photon and the phonon dispersion in the PhC nanowire array.

We used the scattering matrix method [21], with tabulated values for the refractive index of InP [22], for studying the optical eigenmodes of the array. Each eigenmode shows a well-defined propagation vector β in a direction parallel to the axis of the nanowires [17]. For each mode we calculated an effective refractive index $n_{mode} = \beta/(2\pi/\lambda)$, which is presented in Fig. 2. We solved also the dispersion relation for the fundamental HE_{11} waveguide mode of an individual nanowire. The dispersion of this mode agrees very well with that of mode 1 of the array at shorter wavelength. In contrast,

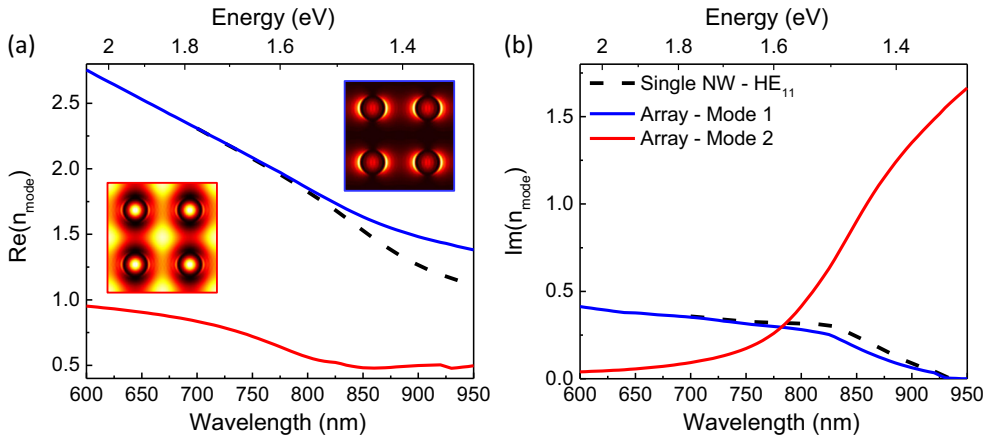

FIG. 2. Dispersion of the two optical modes that show the longest propagation length in a square array of InP nanowires with a diameter of 180 nm at $\lambda = 800$ nm. The period of the array is 400 nm. (a) Real and (b) imaginary part of the effective refractive index of the two optical modes of the nanowire array PhC (full lines). Here we show also the dispersion of the fundamental HE_{11} mode of an individual nanowire of $D = 180$ nm (dashed lines). Inset in (a): Electric field distribution $|\mathbf{E}|^2$ of mode 1 (upper right) and mode 2 (lower left) at 850 nm.

mode 2 of the array does not appear for an individual nanowire. This mode is delocalized from the nanowires and the dispersion relation of this mode is strongly dependent on the array period. It is thus possible to tune the properties of mode 2, without changing the nanowire diameter.

Next, we used the RUS method to calculate the dispersion relations [Fig. 3(a)], and displacement fields [Fig. 3(e)] of the phonons of a single nanowire [16,23]. The frequencies for forward scattering [green arrows in Figs. 1(c) and 3(a)], which correspond to $q_{\text{phonon}} = 0$, can be attributed to the quadrupolar mode [11 GHz, Q in Fig. 3(a)], and the fundamental (19 GHz, B) and higher order (47 GHz, 2B) breathing mode. For the longitudinal mode [L in Fig. 3(a)], the frequency goes to zero at $q = 0$ and therefore does not contribute to forward scattering.

Note that the intensity of the laser spot is almost constant on the length scale of the nanowire diameter, thus one could expect only axisymmetric modes, namely the longitudinal and breathing modes [13,14]. It may therefore seem surprising

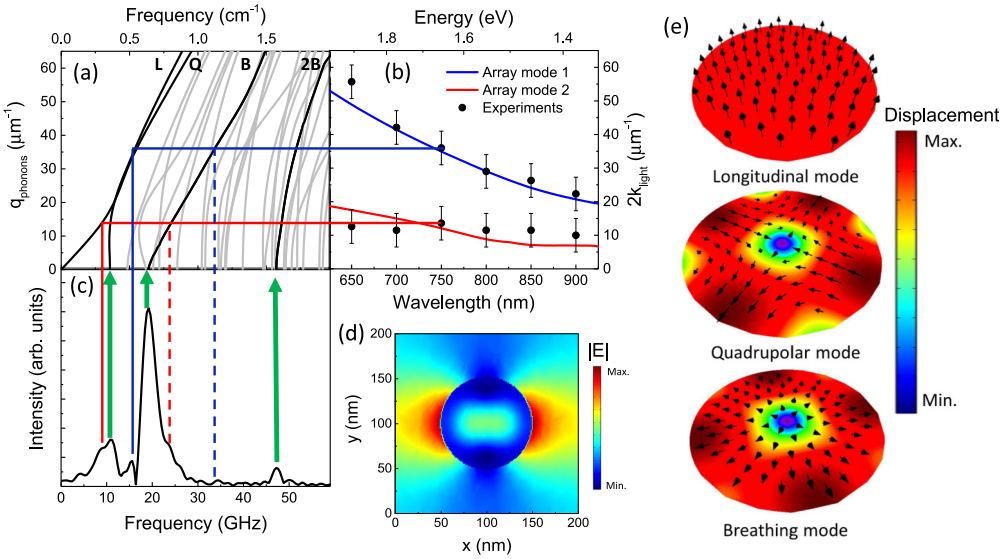

FIG. 3. (a) Phonon dispersion relations in an InP nanowire of 180 nm in diameter. The black lines correspond to the acoustic modes that can be experimentally generated by the pump light. (b) The wave vectors of the optical mode of the array multiplied by a factor 2 as a function of the incident light wavelength. The black circles represent the phonon wave vectors that correspond to the experimental frequencies extracted from the dispersion relation. The error bars are obtained considering the resolution in the Fourier transform, and thus of the wave vectors. (c) Fourier transform of the transient reflectivity traces obtained for $\lambda_{\text{pump}} = 550$ nm and $\lambda_{\text{probe}} = 750$ nm. The green arrows corresponds to the experimental frequencies that remain unchanged when varying probe wavelength, the vertical solid and dashed lines link the experimental frequencies to the acoustic phonon branches of the dispersion relation, and the horizontal lines link the acoustic mode wave vector to the optical mode wave vector. (d) Electric field |E| calculated for a 180 nm diameter InP nanowires, 100 nm beneath the top surface, with an 550 nm, x-polarized incident light. (e) Displacement field of the experimentally observed guided acoustic phonons in single nanowires calculated using the RUS method.

to observe the quadrupolar mode, which corresponds to an expansion along one direction of the nanowire cross section accompanied by a compression in the perpendicular direction [Fig. 3(e)]. However, the polarization of light breaks the circular symmetry and absorption of light becomes nonhomogeneous [Fig. 3(d)] allowing the generation of the quadrupolar mode. This breaking of the circular symmetry of the electric field depends on the wavelength of the incident light and the diameter of the nanowire. Therefore, at a given diameter there exists an optimum wavelength for the generation of the quadrupolar mode.

Concerning backward scattering, we identified two frequencies that shifted with probe wavelength. These frequencies are marked by the red and blue vertical lines in Fig. 3(a). Reporting these frequencies on the phonon dispersion relations of Fig. 3(a) reveals the wave vector of the corresponding phonon modes. We attribute the lower frequency peak to the scattering of light by the longitudinal mode, and the higher frequency peak to the scattering by the longitudinal and the quadrupolar mode. Next, by using the relation $q_{\text{phonons}} = 2k_{\text{light}}$, we can compare the experimental wave vectors [horizontal red and blue lines going into Fig. 3(c)] with the calculated dispersion relation of the optical mode 1 and mode 2 of the PhC. We also notice two peaks at 25 and 33 GHz. By reporting these frequencies on the dispersion relations, we find a good agreement with the backward scattering of the breathing mode. Likewise, in Fig. 1(c) we observe a component at 25 GHz that is in good agreement with the expected frequency of backward Brillouin scattering of the breathing mode. We performed such experiments and analysis for varying probe wavelength [marked by the set of black circles in Fig. 3(c)] and find very good agreement with the predicted dispersion of both mode 1 and mode 2. Thus, we conclude that both mode 1, the guided optical HE_{11} mode in the constituent nanowires, as well as mode 2, the delocalized array mode, contribute to the Brillouin scattering.

Thus, the acoustic phonons that are strongly confined to a single nanowire can interact with a delocalized optical array mode (mode 2). We now investigate the relative scattering of each optical mode with guided phonons. To do so, we simulated the relative excitation of each optical mode as a function of the probe wavelength [Fig. 4(a)]. More specifically, we show here the power carried by each mode, P11++ and P22++, as defined in Appendix C of Ref. [17], at the top surface of the nanowire array and normalized to the incident power flow.

At larger wavelength, mode 1, which is similar to the HE_{11} mode of individual nanowires, is more strongly excited than mode 2. However, when the wavelength is decreased, the array mode 2 becomes predominant. We found, from Fig. 4(a), that at 800 nm for instance, the excitation of mode 1 is approximately two times stronger than that of mode 2. At this wavelength, the backward scattering of mode 2 [red arrow in Fig. 1(c)] is as strong as the backscattering of mode 1 [blue arrow in Fig. 1(c)], as measured by the peak intensity of the Fourier transform. This is an interesting result as it demonstrates that in the array the delocalized mode 2 has enhanced interaction with guided acoustic phonons compared to the localized mode 1. Insight in this enhancement can be obtained by looking at the scattering mechanisms [24]. The coupling of light and sound occurs typically through the photoelastic effect or via the displacement of the nanowire boundary [24]. In the photoelastic effect, the phonons induce a change of refractive index over the full nanowire cross section, thus perturbing light. The second mechanism can be understood as follows: a nanowire of permittivity ε_1 is embedded in a medium of permittivity ε_2. If we consider the cross section, then, when the nanowire boundaries are moving, the area with permittivity ε_1 is modified, creating a perturbation of the electric field. The electric field of mode 1 is strongly localized on the outer surface of the nanowires at 850 [inset of Fig. 2(a)] and 550 nm [Fig. 3(d)]. This mode is thus expected to be sensitive to the moving boundaries mechanism, but weakly to the photoelastic mechanism. On the other hand, the electric field of mode 2 is centered in the nanowires and between them [inset of Fig. 2(a)]. The part of the field centered between the nanowires should not affect the coupling to phonons as it is too far from the boundaries. However, the part centered within the nanowire should be strongly affected by the photoelastic effect. We thus attribute the enhancement of phonon coupling to mode 2 relative to mode 1 to the electric field localization and the stronger influence of the photoelastic mechanism.

As an outlook, the demonstrated interaction of phonons with the delocalized optical mode of the array opens possibilities for tailoring the interaction between light and sound at the nanoscale. By designing the nanowire diameter, we can tune the phonon dispersion. After this, by designing the array period, we can tune the dispersion of the delocalized optical mode without altering the phonon dispersion, as shown in Figs. 4(b) and 4(c). Thus we can independently tune the frequency of the photon and the phonon that interact through Brillouin scattering. Such freedom in the tuning of the frequencies could offer increased flexibility for the design of systems harnessing the potential of Brillouin scattering at the nanoscale. Additionally, the modified electric field of the guided optical mode allows the generation of guided acoustic phonons (like the quadrupolar mode). The access to such additional phonon modes should lead to efficient nondestructive mechanical, optical, and geometric characterization of nanowires.

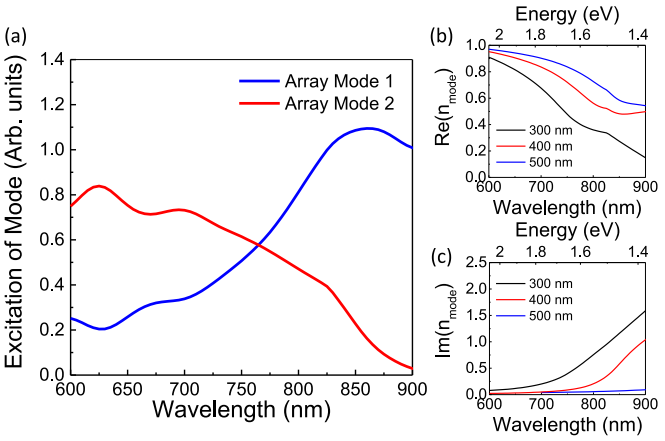

FIG. 4. (a) Excitation of the array optical modes as a function of the incident wavelength. (b) Real and (c) imaginary part of the effective refractive index of the second optical modes of the nanowire array PhC as a function of the period of this array.

In conclusion, we have observed the scattering of light by guided acoustic phonons in a nanowire photonic crystal. We simulated the multiple optical modes that this structure can sustain, revealing both an individual nanowire waveguide mode and a delocalized array optical mode. Using time resolved spectroscopy, we observed both forward and backward Brillouin scattering of the optical modes by the guided acoustic phonons of the individual nanowires, including the enhanced scattering of an array mode that is delocalized from single nanowires. We analyzed the various scattering mechanisms to explain this enhancement. Our results propose a way to tailored light manipulation at the nanoscale.

This work was performed within NanoLund and was supported by NanoLund, the Swedish Research Council VR, the Swedish Foundation for Strategic Research SSF, the Swedish Energy Agency, the People Program of the European Union (Marie Curie Actions, FP7-People-2013-ITN) Grant No. 608153, PhD4Energy, the Crafoord Foundation, and the Knut and Alice Wallenberg Foundation.

[1] W. Hayes and R. Loudon, *Scattering of Light by Crystals* (Wiley, New York, 1978).
[2] P. T. Rakich, C. Reinke, R. Camacho, P. Davids, and Z. Wang, Phys. Rev. X **2**, 011008 (2012).
[3] R. Van Laer, B. Kuyken, D. Van Thourhout, and R. Baets, Nat. Photon. **9**, 199 (2015).
[4] H. Shin, W. Qiu, R. Jarecki, J. A. Cox, R. H. Olsson III, A. Starbuck, Z. Wang, and P. T. Rakich, Nat. Commun. **4**, 1944 (2013).
[5] L. Thevenaz, Nat. Photon. **2**, 474 (2008).
[6] J. D. Cohen, S. M. Meenehan, G. S. MacCabe, S. Gröblacher, A. H. Safavi-Naeini, F. Marsili, M. D. Shaw, and O. Painter, Nature (London) **520**, 522 (2015).
[7] J. Kim, M. C. Kuzyk, K. Han, H. Wang, and G. Bahl, Nat. Phys. **11**, 275 (2015).
[8] C. Thomsen, J. Strait, Z. Vardeny, H. J. Maris, J. Tauc, and J. J. Hauser, Phys. Rev. Lett. **53**, 989 (1984).
[9] P.-A. Mante, C.-C. Chen, Y.-C. Wen, J.-K. Sheu, and C.-K. Sun, Phys. Rev. Lett. **111**, 225901 (2013).
[10] A. Fainstein, N. D. Lanzillotti-Kimura, B. Jusserand, and B. Perrin, Phys. Rev. Lett. **110**, 037403 (2013).
[11] I-J. Chen, P.-A. Mante, C.-K. Chang, S.-C. Yang, H.-Y. Chen, Y.-R. Huang, L.-C. Chen, K.-H. Chen, V. Gusev, and C.-K. Sun, Nano Lett. **14**, 1317 (2014).
[12] C. Brüggemann, A. V. Akimov, A. V. Scherbakov, M. Bombeck, C. Schneider, S. Höfling, A. Forchel, D. R. Yakovlev, and M. Bayer. Nat. Photon. **6**, 30 (2011).
[13] A. Crut, P. Maioli, N. Del Fatti, and F. Vallée, Phys. Rep. **549**, 1 (2015).
[14] C. Jean, L. Belliard, T. W. Cornelius, O. Thomas, M. E. Toimil-Molares, M. Cassinelli, L. Becerra, and B. Perrin, J. Phys. Chem. Lett. **5**, 4100 (2014).
[15] S.-C. Yang, Y.-C. Wu, P.-A. Mante, C.-C. Chen, H.-P. Chen, H.-Y. Chou, M.-H. Shih, and C.-K. Sun, Appl. Phys. Lett. **105**, 243101 (2014).
[16] P.-A. Mante, Y.-C. Wu, Y.-T. Lin, C.-Y. Ho, L.-W. Tu, and C.-K. Sun, Nano Lett. **13**, 1139 (2013).
[17] N. Anttu and H. Q. Xu, Opt. Express **21**, 21, A558 (2013).
[18] A. C. Scofield, S.-H. Kim, J. N. Shapiro, A. Lin, B. Liang, A. Scherer, and D. L. Huffaker, Nano Lett. **11**, 5387 (2011).
[19] T. Mårtensson, P. Carlberg, M. Borgström, L. Montelius, W. Seifert, and L. Samuelson, Nano Lett. **4**, 699 (2004).
[20] M. T. Borgström, J. Wallentin, J. Trägårdh, P. Ramvall, M. Ek, L. R. Wallenberg, and L. Samuelson, Knut Deppert, Nano Res. **3**, 264 (2010).
[21] N. Anttu, Z. Q. Guan, U. Håkanson, H. X. Xu, and H. Q. Xu, Appl. Phys. Lett. **100**, 091111 (2012).
[22] O. J. Glembocki and H. Piller, in *Handbook of Optical Constants of Solids*, edited by E. D. Palik (Academic, New York, 1997).
[23] N. Nishiguchi, Y. Ando, and M. N. Wybourne, J. Phys.: Condens. Matter **9**, 5751 (1997).
[24] C. Wolff, M. J. Steel, B. J. Eggleton, and C. G. Poulton, Phys. Rev. A **92**, 013836 (2015).